Original Article

Whole-section digital analysis of immune profiles in surgically resected small cell lung carcinoma and their associations with molecular subtypes

Yanli Zhu[1#], Jianghua Wu[1#], Haiyue Wang[1#], Kaiwen Chi[1], Xinting Diao[1], Minglei Zhuo[2], Dongmei Lin[1]

[1]Key Laboratory of Carcinogenesis and Translational Research (Ministry of Education), Department of Pathology, Peking University Cancer Hospital and Institute, Beijing, China; [2]Key Laboratory of Carcinogenesis and Translational Research (Ministry of Education), Department I of Thoracic Oncology, Peking University Cancer Hospital and Institute, Beijing, China

Contributions: (I) Conception and design: Y Zhu, M Zhuo, D Lin; (II) Administrative support: None; (III) Provision of study materials or patients: K Chi, X Diao; (IV) Collection and assembly of data: Y Zhu, H Wang, K Chi; (V) Data analysis and interpretation: Y Zhu, J Wu, H Wang; (VI) Manuscript writing: All authors; (VII) Final approval of manuscript: All authors.

[#]These authors contributed equally to this work.

Correspondence to: Dongmei Lin, MD. Key Laboratory of Carcinogenesis and Translational Research (Ministry of Education), Department of Pathology, Peking University Cancer Hospital and Institute, No. 52 Fu-Cheng Road, Haidian District, Beijing 100142, China. Email: lindm3@bjmu.edu.cn; Minglei Zhuo, MD. Key Laboratory of Carcinogenesis and Translational Research (Ministry of Education), Department I of Thoracic Oncology, Peking University Cancer Hospital and Institute, No. 52 Fu-Cheng Road, Haidian District, Beijing 100142, China. Email: minglei1978@163.com.

Background: The molecular subtype-specific features of the tumor immune microenvironment (TIME) in small cell lung carcinoma (SCLC) remain poorly understood. We aimed to analyze the immune profiles in surgically resected SCLC and their associations with molecular subtypes.

Methods: Tumor samples from 83 treatment-naive SCLC patients who underwent surgical resection were analyzed. The protein expression of subtype-defining markers (ASCL1, NEUROD1, POU2F3, and YAP1) and nine immune-related markers were assessed using whole-section immunohistochemistry. Digital image analysis was employed for precise quantification of immune cell infiltrates and distributions. The findings were subsequently correlated with clinicopathological parameters and patient prognoses.

Results: Unsupervised hierarchical clustering categorized the tumors into four molecular subtypes: achaete-scute homologue 1-dominant (ASCL1; SCLC-A, 71.1%, n=59), neuronal differentiation factor 1-dominant (NEUROD1; SCLC-N, 12.1%, n=10), POU class 2 homeobox 3-dominant (POU2F3; SCLC-P, 10.8%, n=9), and quadruple-negative (SCLC-QN, 6.0%, n=5). Expression of major histocompatibility complex class I (MHC I) and class II (MHC II; P=0.02, P=0.02), tumor programmed death-ligand 1 (PD-L1; P=0.006), and an inflamed phenotype characterized by $CD8^+$/$CD3^+$ T cells (P=0.001, P=0.003) were more prominent in SCLC-P tumors compared to other subtypes. Additionally, SCLC-P tumors demonstrated the highest levels of MHC II (P=0.04) and PD-L1 expression on both tumor and stromal cells (P=0.003, P=0.01). The tumor proportion score of PD-L1 positively correlated with tumor expression levels of POU2F3 (rho=0.297, P=0.006) and MHC I (rho=0.239, P=0.03), as well as the combined positive score of PD-L1 (rho=0.222, P=0.04; rho=0.433, P<0.001). Intra-tumoral tertiary lymphoid structures (intra-TLS) and peri-tumoral TLS (peri-TLS) were observed in 60.2% (n=50) and 96.4% (n=80) of patients, respectively. High intra-TLS density was more frequently associated with SCLC-P tumors (P=0.02). Notably, low peri-TLS density and stromal PD-L1 expression were linked to improved overall survival (OS) and progression-free survival (PFS), respectively.

Conclusions: This study highlights the heterogeneity of the TIME across molecular subtypes of SCLC. The SCLC-P subtype and MHC I expression may serve as predictive biomarkers for immunotherapy response, while peri-TLS density and stromal PD-L1 expression might serve as prognostic indicators in resected SCLC.

Keywords: Small cell lung carcinoma (SCLC); molecular subtype; tumor immune microenvironment (TIME); digital pathology; tertiary lymphoid structure (TLS)

Submitted Oct 08, 2024. Accepted for publication Jan 09, 2025. Published online Feb 27, 2025.
doi: 10.21037/tlcr-24-924
View this article at: https://dx.doi.org/10.21037/tlcr-24-924

Introduction

Small cell lung carcinoma (SCLC) is a high-grade neuroendocrine neoplasm, with a dismal 5-year overall survival rate of only 6% (1). Recently, immune checkpoint inhibitors (ICIs)-based immunotherapy targeting programmed cell death protein 1 (PD-1), or its ligand, programmed death-ligand 1 (PD-L1), has been introduced as frontline therapy for SCLC. However, ICIs have led to only modest improvements in overall survival (2,3). Despite this, recent clinical trials have consistently reported a subset of SCLC patients who derive significant and durable benefits from immunotherapy (4,5). Identifying predictive biomarkers is therefore crucial to pinpoint the small population of SCLC patients most likely to respond favorably to ICIs. Furthermore, a comprehensive analysis of the immune landscape within the tumor microenvironment is urgently needed, as the tumor immune microenvironment (TIME) may play a critical role in determining the efficacy of ICIs (6).

Recent profiling studies of SCLC have identified molecular subtypes based on the relative expression profiles of four key transcriptional regulators: achaete-scute homologue 1 (ASCL1; SCLC-A), neuronal differentiation factor 1 (NEUROD1; SCLC-N), POU class 2 homeobox 3 (POU2F3; SCLC-P) and Yes-associated protein 1 (YAP1; SCLC-Y), and each subtype exhibits distinct molecular characteristics and specific therapeutic vulnerabilities (7). The neuroendocrine (NE) phenotype, encompassing SCLC-A and SCLC-N, accounts for approximately 80% of all SCLCs and is generally associated with immune desert properties. In contrast, non-NE SCLCs (approximately 20%), are more likely to exhibit immune oasis properties (8). However, the role of YAP1 as a defining marker for SCLC remains controversial, as its expression is typically absent or minimal (9-12). Consequently, a new subtype, SCLC-I, has been proposed, characterized by high expression of inflammatory genes, including multiple immune checkpoints and human lymphocyte antigens (9). Retrospective analyses from the IMpower133 and CASPIAN trials revealed that patients with SCLC-I tumors exhibited higher overall survival rates with immunotherapy compared to other subtypes (9,13). Recent studies have further highlighted the immunogenic nature of POU2F3. Best *et al.* reported that the T cell scores were highest in the POU2F3 subset (14). Similarly, Chen *et al.* demonstrated that among 10 genes used to predict the SCLC-I subtype, POU2F3 was the most significantly upregulated gene with high expression. Furthermore, POU2F3 protein level was

Highlight box

Key findings

- Major histocompatibility complex class I (MHC I)/MHC II expression, tumor programmed death-ligand 1 (PD-L1) expression, and an inflamed phenotype of $CD8^+/CD3^+$ T cells were more frequently observed in the POU2F3-dominant small cell lung carcinoma (SCLC-P) tumor compared to other molecular subtypes.
- Tumor proportion score of PD-L1 was positively correlated with tumor expression levels of POU2F3 and MHC I, as well as the combined positive score of PD-L1.
- High intra-tumoral tertiary lymphoid structure (intra-TLS) density was predominantly associated with the SCLC-P subtype. Additionally, low peri-tumor TLS (peri-TLS) density and stromal PD-L1 expression were linked to improved OS and PFS, respectively.

What is known and what is new?

- The clinical application of immunotherapy in SCLC remains challenging, with no reliable predictive biomarkers identified to date. Moreover, the molecular subtype-specific features of the tumor immune microenvironment (TIME) in SCLC are poorly understood.
- Our study validated the heterogeneity of TIME across SCLC molecular subtypes and suggested that the SCLC-P subtype and MHC I expression may serve as predictive biomarkers for immunotherapy efficacy.

What is the implication, and what should change now?

- By analyzing the TIME of SCLC using whole-slide image-based digital pathology, our findings provide a foundation for future hypothesis-driven validation studies. These results may inform the development of subtype-specific immunotherapy strategies and guide future research into predictive biomarkers for SCLC.

positively correlated with improved prognosis in patients receiving immunotherapy or chemo-immunotherapy (15). In contrast, data from the IMpower133 trial suggested that the SCLC-P subtype might represent a poor prognostic marker for immunotherapy compared to the other subtypes (9). Interestingly, it has been reported that immune-inflamed subsets can exist within both NE and non-NE phenotypes (16), and the inflamed phenotype appears across molecular subtypes with varying prevalence (17). Collectively, these findings highlight a potential correlation between molecular subtypes and the TIME in SCLC. However, this relationship remains unclear. A comprehensive analysis of the TIME characteristics within each molecular subtype is essential to elucidate the precise link between these subtypes and their responsiveness to immunotherapy.

In this study, we collected surgically resected primary samples from untreated SCLC patients and analyzed the protein expression of four molecular subtype markers (ASCL1, NEUROD1, POU2F3 and YAP1) as well as four immunotherapy-related markers, including major histocompatibility complex class I (MHC I), major histocompatibility complex class II (MHC II), PD-L1 and retinoblastoma (Rb) (18-21), using immunohistochemistry (IHC). In addition, we evaluated immune cell infiltration in the stroma and tumor nests using several immune biomarkers, including CD3, CD4, CD8, CD20 and CD68. To address the potential inaccuracies of manual analysis, we employed whole-slide images-based digital pathology, a method that has been validated in multiple studies to provide precise quantification of immune cell infiltrates in IHC-stained sections (22,23). Finally, survival analysis was conducted to investigate the relationship between clinicopathologic parameters, including molecular subtypes and TIME features, and patient outcomes. We present this article in accordance with the REMARK reporting checklist (available at https://tlcr.amegroups.com/article/view/10.21037/tlcr-24-924/rc).

Methods

Patient selection and data collection

This retrospective study included surgically resected SCLC specimens from Peking University Cancer Hospital, collected between January 2010 and December 2021. A total of 83 SCLC patients were enrolled, with the following inclusion criteria: (I) pathologically diagnosed with pure SCLC; (II) no preoperative neoadjuvant treatment; (III) accessible tumor tissues with a size ≥0.5 cm, and absence of background lung diseases (e.g., smoking-related pneumonia and interstitial pneumonia); (IV) availability of clinical and pathologic data, including progression-free survival (PFS) and overall survival (OS) data, which were either retrieved from electronic medical records or obtained via telephone interviews. This study was approved by the Ethics Committee of Peking University Cancer Hospital (2023KT23). Given the retrospective design, informed consent from patients was not required, and all patient data was kept confidential. The study was conducted in accordance with the Declaration of Helsinki (as revised in 2013).

All archival slides, including a panel of immunohistochemical markers for the differential diagnosis [TTF-1, Napsin A, P40, CK5/6, LCA, CD56, CgA, Syn, NUT, INI-1 and SMARCA4 (BRG1)], were independently reviewed by two senior pathologists (Y.Z. and H.W.) to confirm the diagnosis of pure SCLC. Discrepant cases were resolved through consensus using a multiheaded microscope. Tumors were staged according to the 8th edition of the American Joint Committee on Cancer (AJCC) tumor-node-metastasis (TNM) classification (24).

IHC staining and digital image analysis

Formalin-fixed, paraffin-embedded specimens were prepared, and consecutive 4-μm-thick tissue sections were cut for IHC analysis. All samples were stained for molecular subtype markers (ASCL1, NEUROD1, POU2F3 and YAP1) as described in our previous study (25), as well as a panel of nine TIME related markers: MHC I, MHC II, PD-L1, Rb, CD3, CD4, CD8, CD20 and CD68. Detailed IHC protocols are summarized in Table S1. All IHC analyses were evaluated by two experienced observers (Y.Z. and H.W.), who were blinded to the patients' clinical data.

For molecular subtype markers and MHC I/II, a histoscore (H-score) was calculated. The entire tumor area of each specimen was evaluated, and marker expression was quantified using the H-score, which was derived by multiplying the percentage of positivity cells by the intensity score (ranging from 1 to 3), and this method yielded an H-score range of 0–300 (26). As previously reported, an H score ≤10 was considered negative, while an H-score >10 was considered positive (27). To classify SCLC molecular subtypes, unsupervised hierarchal clustering using the Complex Heatmap R package (R version 3.6.3) was performed based on the H-score expression levels of

the four subtype-defining transcription factors (ASCL1, NEUROD1, POU2F3, and YAP1). For Rb, IHC was classified as negative/mutant-type (complete absence of nuclear expression) or positive/wild-type (normal, variable nuclear expression).

Special attention was given to the interpretation of PD-L1 status, as the 22C3 clone is an approved companion diagnostic antibody in clinic practice, based on a mixture of tumor and immune cell expression. Consequently, both tumor and stromal-infiltrating immune cell expressions were evaluated for PD-L1 protein expression. Positivity was defined as PD-L1 expression ≥1% in either tumor cells or immune cells (28). Additionally, the tumor proportion score (TPS) and the combined positive score (CPS) of PD-L1 were assessed. TPS was calculated as the percentage of at least 100 viable cancer cells exhibiting partial or complete membrane staining, while CPS was defined as the ratio of all PD-L1-expressing cells (tumor cells, lymphocytes, macrophages) to the total number of tumor cells (29). During evaluations, alveolar macrophages, which frequently express PD-L1, and areas of necrosis were excluded from analysis.

Immunostaining for CD3, CD4, CD8, CD20 and CD68 was captured at 200× magnification using the Pannoramic 250 Flash III scanner (3DHISTECH, Budapest, Hungary) and quantified by absolute cell count with QuPath (version 0.5.1), detecting 3,30-diaminobenzidine (DAB)-positive cells (30). Whole-slide imaging was classified into three regions: "tumor" (within the mass of tumor cells), "stroma" (non-cancer cells adjacent to tumor cells) and "region" (the area within 2 millimeters of the leading edge of the tumor). Classification was performed using user-defined examples and QuPath's machine learning features, as described previously (30). The number of positive cells in each region was then counted, and results from the whole-slide imaging were averaged prior to statistical assessment. Further classification into low and high densities of immune cells was performed based on the median cell density as the cut-off point.

Additionally, tumors were categorized into immunophenotypes based on the presence and pattern of immune cell infiltration relative to tumor cells. These immunophenotypes were defined as follows: "desert", characterized by low prevalence of immune cells; "excluded", when immune cells were predominantly found in the stroma adjacent to or within the tumor; and "inflamed", when immune cells were in direct contact with tumor cells, either as spillover from stromal infiltrates into tumor cell aggregates or as diffuse infiltration of tumor cells (Figure S1) (31).

Finally, the presence and localization of tertiary lymphoid structures (TLSs) were evaluated. TLSs are characterized by clusters of B-cell follicles surrounded by T cells, and their existence and structure were confirmed by IHC staining: CD20 marked the B-cell area, and CD3 marked the T-cell area (*Figure 1A-1D*). Tumors with at least one TLS were classified as TLS-positive, while those without any TLS were classified as TLS-negative. Based on their distribution, TLSs were divided into intra-tumoral TLS (intra-TLS) and peritumoral TLS (peri-TLS). Intra-TLS and peri-TLS were further categorized into low and high sets. High intra-TLS was defined as the presence of at least three TLSs within the tumor areas, while high peri-TLS referred to a TLS distribution spanning more than 50% of the peritumoral region or extensive TLS infiltration across the entire peritumoral region (*Figure 1E-1L*) (32).

Statistical analysis

Data visualization and statistical analysis were performed using SPSS software (version 26.0; SPSS Inc., USA) and Prism version 8.0 (GraphPad Software, San Diego, CA, USA). Categorical variables are presented as numbers and percentages, while continuous variables are presented as ranges and medians. Associations between categorical variables were analyzed using the χ^2 test or Fisher's exact test. For non-parametric variables, Kruskal-Wallis or Mann-Whitney *U* tests were applied. Spearman's correlation was used to assess the strength and direction of the linear relationship between two continuous variables. OS was calculated from the date of pathological diagnosis to the date of death, while PFS was calculated from the date of pathological diagnosis to the date of the last clinical evidence of recurrence, progression, or death. Univariable and multivariable Cox proportional hazards regression analyses were conducted to evaluate the hazard ratio and 95% confidence interval of risk factors. Kaplan-Meier survival curves and log-rank tests were used to compare the survival difference between two or more groups. A two-sided P value <0.05 was considered statistically significant.

Results

Patient and sample characteristics

A total of 83 patients with SCLC were included in this study. As shown in *Table 1*, the median patient age of

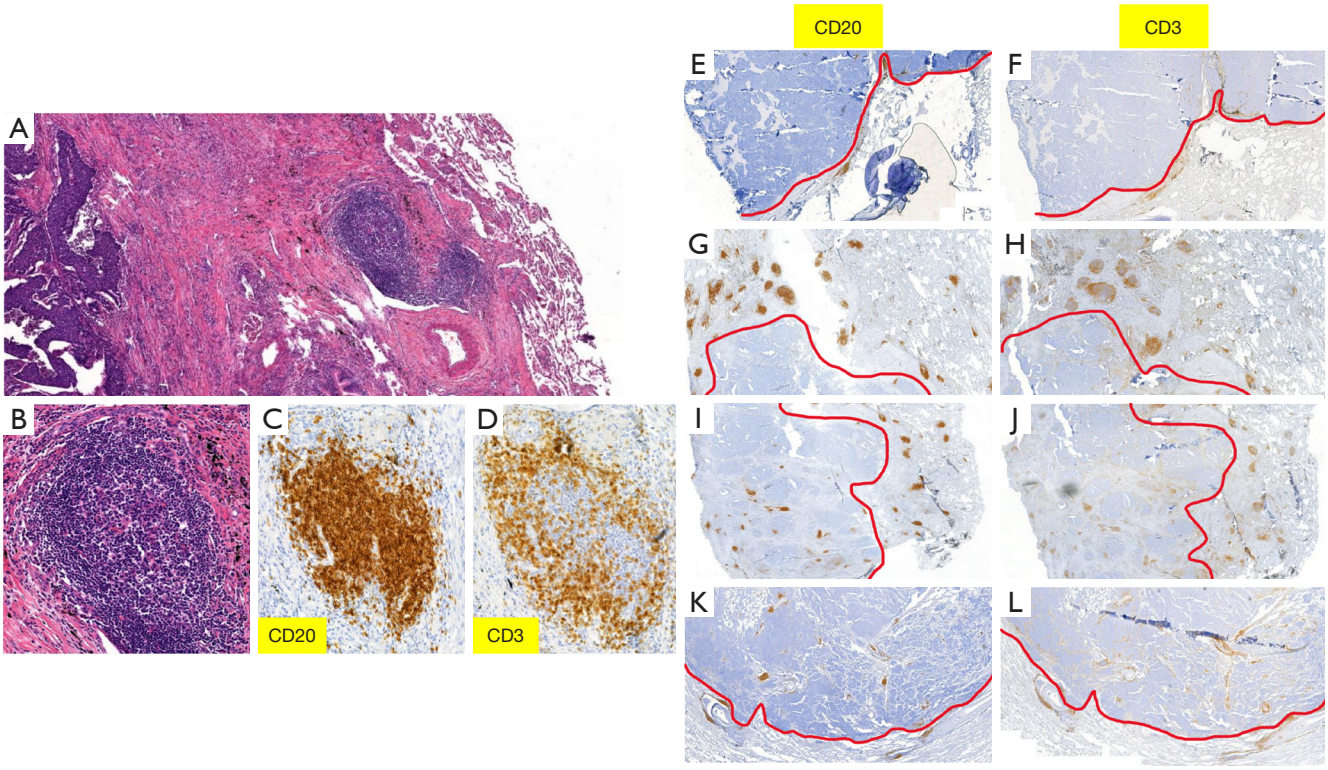

Figure 1 Characteristics of TLSs. (A) H&E-stained SCLC tissue showing a peri-TLS (magnification: ×50). (B) A representative TLS assessed in H&E sections (magnification: ×150). (C) The B-cell zone of the TLS, marked by CD20 expression in IHC sections (magnification: ×150). (D) The T-cell zone of the TLS, marked by CD3 expression in IHC sections (magnification: ×150). (E,F) Representative images of a case with low intra-TLS and low peri-TLS in IHC sections (magnification: ×20). (G,H) Representative images of a case with low intra-TLS and high peri-TLS in IHC sections (magnification: ×20). (I,J) Representative images of a case with high intra-TLS and high peri-TLS in IHC sections (magnification: ×20). (K,L) Representative images of a case with high intra-TLS and low peri-TLS in IHC sections (magnification: ×20). The red lines in (E-L) were drawn by us, suggesting the boundary between tumor and the invasive frontier. SCLC, small cell lung carcinoma; TLS, tertiary lymphoid structure; intra-TLS, intra-tumoral tertiary lymphoid structure; peri-TLS, peri-tumoral tertiary lymphoid structure; H&E, hematoxylin and eosin; IHC, immunohistochemistry.

the patients was 60.1 years (range, 33–82 years). Of the patients, 58 (69.9%) were men, and 9 (10.8%) were never-smokers with *de novo* SCLC. No patients had histologic transformation after treatment with tyrosine kinase inhibitors (TKIs). Among the patients, 5 (6.0%) had central tumors, while 78 (94.0%) had peripheral tumors. The disease stages were distributed as follows: 45 (54.2%) patients had stage I, 21 (25.3%) had stage II and 17 (20.5%) had stage III disease. After surgical resection, 48 (57.8%) patients received postoperative chemotherapy, 35 (42.2%) received postoperative radiotherapy, and 35 (42.2%) received prophylactic cranial irradiation (PCI).

Molecular subtypes

The positive expression rates of the four molecular subtype markers—ASCL1, NEUROD1, POU2F3 and YAP1—were 78.3%, 26.5%, 12.0% and 16.9%, respectively. In addition to the previously identified SCLC-A (ASCL1-dominant), SCLC-N (NEUROD1-dominant), and SCLC-P (POU2F3-dominant), unsupervised hierarchical clustering analysis revealed a fourth subtype, the quadruple-negative SCLC subtype (SCLC-QN), characterized by the low expression of all four subtype-specific proteins (*Figure 2A*). Among the patients, 71.1% (n=59) were categorized as SCLC-A, 12.1% (n=10) as SCLC-N, 10.8% (n=9) as

Table 1 Demographics of the included patients and samples

Parameter	Value
Age (years), median [range]	61 [33–82]
Sex, n (%)	
Male	58 (69.9)
Female	25 (30.1)
Smoking history, n (%)	
Yes	74 (89.2)
No	9 (10.8)
Tumor location, n (%)	
Central	5 (6.0)
Peripheral	78 (94.0)
TNM stage, n (%)	
I	45 (54.2)
II	21 (25.3)
III	17 (20.5)
Postoperative chemotherapy, n (%)	
Yes	48 (57.8)
No	35 (42.2)
Postoperative radiotherapy, n (%)	
Yes	35 (42.2)
No	48 (57.8)
Prophylactic cranial irradiation, n (%)	
Yes	35 (42.2)
No	48 (57.8)

TNM, tumor-node-metastasis.

SCLC-P, and 6.0% (n=5) as SCLC-QN. Representative histopathological images of the marker-defined SCLC molecular subtypes are shown in *Figure 2B*, and the clinical and TIME characteristics of each molecular subtype are summarized in *Table 2*.

Expression of MHC I, MHC II, PD-L1 and Rb in different molecular subtypes

The expression of MHC I and MHC II on tumor cells was assessed in 83 SCLC samples. Forty-seven samples (56.6%%) were positive for MHC I, and seventeen samples (20.5%) were positive for MHC II. The expression rates of both MHC I and MHC II were highest in the SCLC-P subtype, with significant differences compared to other molecular subtypes (P=0.02, P=0.02) (*Table 2*). Moreover, the expression level of MHC II was the strongest in the SCLC-P subtype among all four molecular subtypes (P=0.04) (*Figure 3A*).

Next, PD-L1 protein expression was evaluated on both tumor cells and stromal-infiltrating immune cells. The range of TPS and CPS values for PD-L1 in this cohort were 0–80% and 0–90, respectively. The positive expression rate of PD-L1 on tumor cells was 15.7% (13/83), while PD-L1 expression on the stromal cells was more prevalent, occurring in 53.0% (44/83) of samples. This difference in expression between tumor and stromal cells was statistically significant (P<0.001). A significant correlation was observed between positive tumor PD-L1 expression and the SCLC-P subtype compared to the other molecular subtypes (P=0.006) (*Table 2*). Additionally, the expression level of PD-L1 on both tumor and stromal cells were strongest in the SCLC-P subtype (P=0.003, P=0.01) (*Figure 3B*,*3C*).

For Rb expression, six cases were classified as positive/wild-type. However, no significant difference in Rb expression were observed among the four molecular subtypes (P>0.99) (*Table 2*). Moreover, there were no significant differences in the expression of MHC I among the four molecular subtypes (Figure S2).

Correlation of molecular subtyping and MHC I, MHC II, PD-L1 and Rb expression

We first analyzed the relationship between the expression level of subtype-specific protein and MHC I, MHC II, PD-L1, and Rb expression. Significant positive correlations were found between ASCL1 and the TPS of PD-L1 (rho=–0.305, P=0.005), between POU2F3 and the TPS of PD-L1 (rho=0.297, P=0.006), between POU2F3 and the CPS of PD-L1 (rho=0.222, P=0.04), and between YAP1 and the TPS of PD-L1 (rho=0.349, P=0.001) (*Figure 3D-3G*). No significant correlations were observed between the other groups (Figure S3).

Given the MHC I and MHC II molecules play key roles in antigen presentation and immunological crosstalk within the tumor microenvironment, we further evaluated the association between the expression of MHC I/II and other immune-related markers. Expression levels of MHC I were positively correlated with TPS of PD-L1 (rho=0.239, P=0.03), and CPS of PD-L1 (rho=0.433, P<0.001)

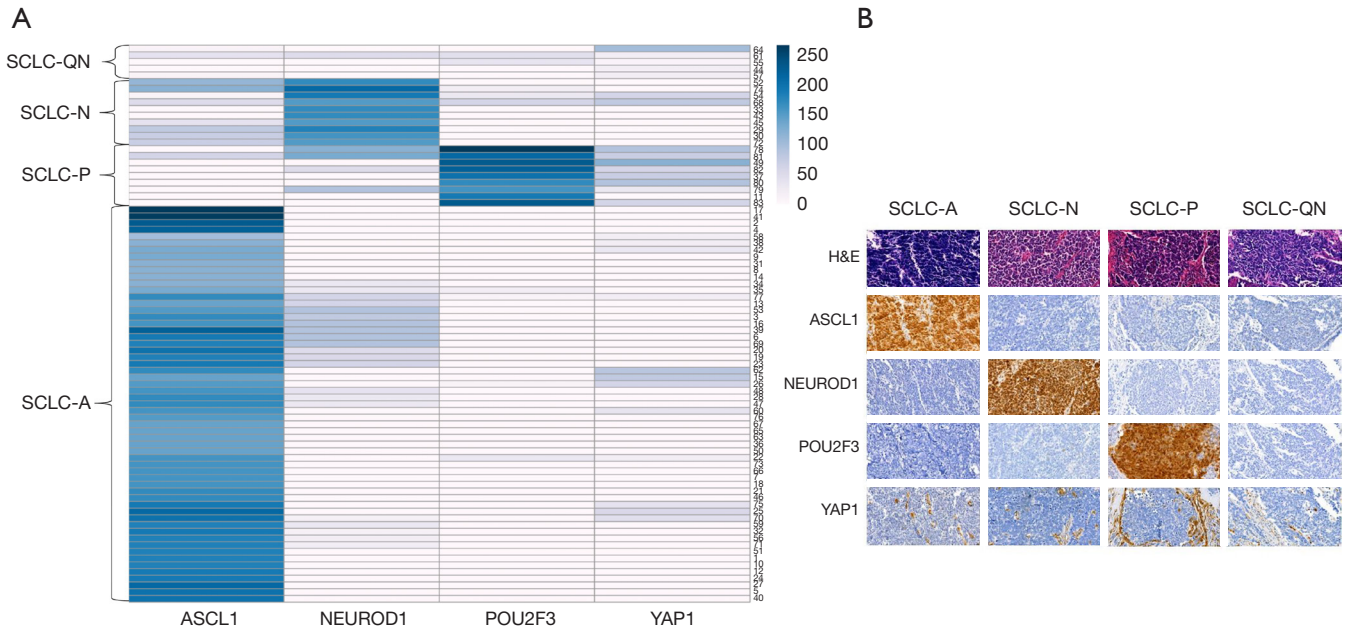

Figure 2 Molecular subtypes distribution. (A) Unsupervised hierarchical clustering identified four molecular subtypes in SCLC: SCLC-A (ASCL1-dominant), SCLC-N (NEUROD1-dominant), SCLC-P (POU2F3-dominant), and a fourth subtype, SCLC-QN, characterized by low expression of all four subtype-specific proteins. (B) Representative histopathological images of SCLC tumors classified by molecular subtypes (magnification: ×400). SCLC, small cell lung carcinoma; ASCL1, achaete-scute homologue 1; NEUROD1, neuronal differentiation 1; POU2F3, POU class 2 homeobox 3; SCLC-QN, quadruple-negative SCLC subtype.

(*Figure 3H-3J*). However, no significant correlation was found between MHC II expression and PD-L1 expression (Figure S3). Additionally, we compared the expression of TIME markers based on the positive or negative results for MHC I and MHC II expressions. Significant differences were observed in the positive rate of PD-L1 expression and $CD8^+$ immune inflamed between the MHC I-positive and MHC I-negative groups (*Table 3*).

Comparison of immunophenotypes among the SCLC tumors grouped by molecular subtypes

Tumors were categorized into immunophenotypes—"desert", "excluded", and "inflamed"—based on the presence of immune cells and their infiltration patterns relative to tumor cells. Tumors with an inflamed phenotype often show better responses to therapy. In our analysis, $CD68^+$ phagocytes were most prevalent in the inflamed phenotype (51.8%), followed by $CD8^+$ T cells (38.6%), $CD3^+$ T cells (27.7%) and $CD4^+$ T cells (25.3%). Notably, no inflamed phenotype was observed in $CD20^+$ B cells.

We then examined the association between molecular subtypes and tumor-associated immunophenotypes of these immune cells. The inflamed phenotype of $CD8^+$ T cells was more commonly observed in the SCLC-P subtype compared to the other molecular subtypes (P=0.001). Similarly, a significant positive correlation was found between the inflamed phenotype of $CD3^+$ T cells and the SCLC-P subtype (P=0.003). However, no significant differences in the immunophenotypes of other immune cells ($CD4^+$, $CD20^+$, and $CD68^+$) were observed across molecular subtypes (*Table 2*).

Immune cells infiltration density and spatial distribution

Digital pathology quantification of CD3, CD4, CD8, CD20, and CD68 expression revealed that, in the TIME of resected SCLC, the highest density of immune cells was found in the invasive margin of the tumors, with relatively few immune cells infiltrating the tumor interior. Among the immune cell types, region $CD20^+$ B cells density was the highest, followed by region $CD4^+$ T cells. In contrast, the density of tumor $CD20^+$ B cells and tumor $CD4^+$ T cells was relatively lower (*Figure 4A*). Next, we analyzed the

Table 2 Clinical and tumor immune microenvironment characteristics of each molecular subtype in small cell lung carcinoma

Parameter	SCLC-A	SCLC-N	SCLC-P	SCLC-QN	P value
Sex					0.13
Male	42 (71.2)	4 (40.0)	8 (88.9)	4 (80.0)	
Female	17 (28.8)	6 (60.0)	1 (11.1)	1 (20.0)	
Age (years)					0.77
≤60	30 (50.8)	5 (50.0)	3 (33.3)	3 (60.0)	
>60	29 (49.2)	5 (50.0)	6 (66.7)	2 (40.0)	
Smoking history					0.09
Yes	55 (93.2)	7 (70.0)	8 (88.9)	4 (80.0)	
No	4 (6.8)	3 (30.0)	1 (11.1)	1 (20.0)	
TNM stage					0.49
I	31 (52.5)	4 (40.0)	6 (66.7)	4 (80.0)	
II–III	28 (47.5)	6 (60.0)	3 (33.3)	1 (20.0)	
MHC I expression					0.02*
Negative	29 (49.2)	2 (20.0)	1 (11.1)	4 (80.0)	
Positive	30 (50.8)	8 (80.0)	8 (88.9)	1 (20.0)	
MHC II expression					0.02*
Negative	47 (79.7)	10 (100.0)	4 (44.4)	5 (100.0)	
Positive	12 (20.3)	0 (0)	5 (55.6)	0 (0)	
Tumor PD-L1 expression					0.006*
Negative	54 (91.5)	8 (80.0)	4 (44.4)	4 (80.0)	
Positive	5 (8.5)	2 (20.0)	5 (55.6)	1 (20.0)	
Stroma PD-L1 expression					0.14
Negative	30 (50.8)	5 (50.0)	1 (11.1)	3 (60.0)	
Positive	29 (49.2)	5 (50.0)	8 (88.9)	2 (40.0)	
Rb expression					>0.99
Negative	54 (91.5)	9 (90.0)	9 (100.0)	5 (100.0)	
Positive	5 (8.5)	1 (10.0)	0 (0)	0 (0)	
CD3 immunophenotypes					0.003*
Immune desert	10 (16.9)	2 (20.0)	0 (0)	0 (0)	
Immune excluded	38 (64.4)	6 (60.0)	1 (11.1)	3 (60.0)	
Immune inflamed	11 (18.6)	2 (20.0)	8 (88.9)	2 (40.0)	
CD4 immunophenotypes					0.96
Immune desert	6 (10.2)	0 (0)	0 (0)	0 (0)	
Immune excluded	39 (66.1)	7 (70.0)	6 (66.7)	4 (80.0)	
Immune inflamed	14 (23.7)	3 (30.0)	3 (33.3)	1 (20.0)	

Table 2 (*continued*)

Table 2 (*continued*)

Parameter	SCLC-A	SCLC-N	SCLC-P	SCLC-QN	P value
CD8 immunophenotypes					0.001*
Immune desert	16 (27.1)	3 (30.0)	0 (0)	2 (40.0)	
Immune excluded	26 (44.1)	4 (40.0)	0 (0)	0 (0)	
Immune inflamed	17 (28.8)	3 (30.0)	9 (100.0)	3 (60.0)	
CD20 immunophenotypes					0.48
Immune desert	23 (39.0)	5 (50.0)	2 (22.2)	3 (60.0)	
Immune excluded	36 (61.0)	5 (50.0)	7 (77.8)	2 (40.0)	
Immune inflamed	0 (0)	0 (0)	0 (0)	0 (0)	
CD68 immunophenotypes					0.79
Immune desert	5 (8.5)	2 (20.0)	0 (0)	0 (0)	
Immune excluded	23 (39.0)	3 (30.0)	5 (55.6)	2 (40.0)	
Immune inflamed	31 (52.5)	5 (50.0)	4 (44.4)	3 (60.0)	
TLS					0.50
Absent	7 (11.9)	2 (20.0)	2 (22.2)	0 (0)	
Present	52 (88.1)	8 (80.0)	7 (77.8)	5 (100.0)	
Intra-TLS density					0.02*
Low	42 (71.2)	10 (100.0)	4 (44.4)	5 (100.0)	
High	17 (28.8)	0 (0)	5 (55.6)	0 (0)	
Peri-TLS density					0.31
Low	31 (52.5)	6 (60.0)	2 (22.2)	3 (60.0)	
High	28 (47.5)	4 (40.0)	7 (77.8)	2 (40.0)	
Stroma CD4 density					0.01*
Low	24 (40.7)	9 (90.0)	5 (55.6)	4 (80.0)	
High	35 (59.3)	1 (10.0)	4 (44.4)	1 (20.0)	

Data are presented as n (%). *, significant P values. SCLC, small cell lung carcinoma; SCLC-A, small cell lung carcinomas with ASCL1 dominant expression; SCLC-N, small cell lung carcinomas with NEUROD1 dominant expression; SCLC-P, small cell lung carcinomas with POU2F3 dominant expression; SCLC-QN, small cell lung carcinomas characterized by the low expression of all four investigated transcription factors; TNM, tumor-node-metastasis; MHC I, major histocompatibility complex class I; MHC II, major histocompatibility complex class II; PD-L1, programmed death-ligand; Rb, retinoblastoma; TLS, tertiary lymphoid structure; intra-TLS, intra-tumoral tertiary lymphoid structure; peri-TLS, peri-tumoral tertiary lymphoid structure.

spatial distribution of immune cells in tumor nests versus stroma. Statistically significant differences were observed in the density of $CD3^+$, $CD4^+$, $CD8^+$, $CD20^+$, and $CD68^+$ cells between the tumor and stroma. The density of all these immune markers was higher in the SCLC tumor stroma than in the tumor interior (*Figure 4B*). The *Figure 4C* further demonstrates that the stroma of tumors is more extensively infiltrated by these immune cells compared to tumor nests.

Additionally, we compared immune cells counts in SCLC tumors grouped by molecular subtype markers and found no significant differences in the density of these immune markers across the different molecular subtypes of SCLC (Figure S2). No significant correlations were detected between immune marker density and subtype-specific protein expression (Figure S4). Significant positive

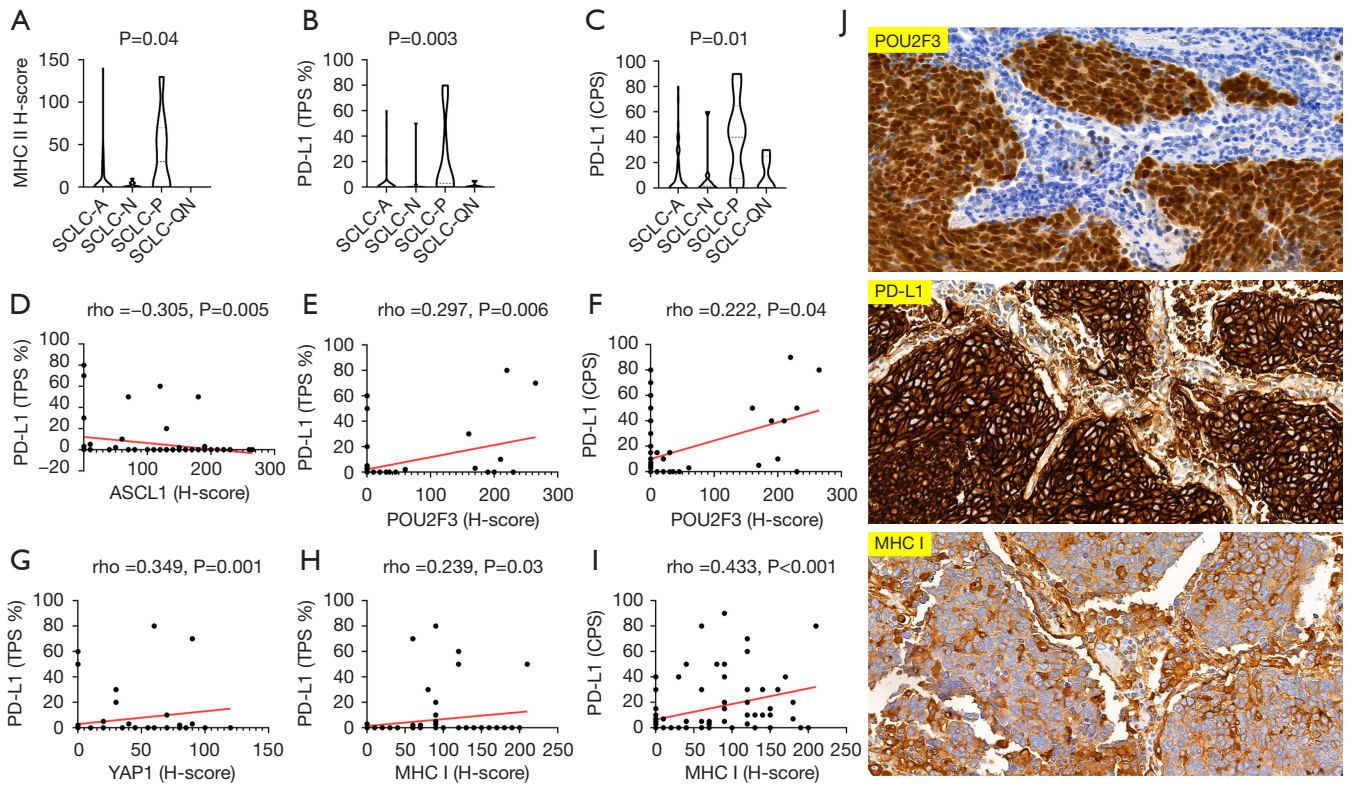

Figure 3 Expression of MHC I, MHC II, PD-L1 and Rb and their correlations with molecular subtypes. (A-C) The expression level of MHC II and PD-L1 were highest in the SCLC-P subtype compared to the other molecular subtypes. (D-G) Significant positive correlations were observed between ASCL1 and PD-L1 TPS (rho=-0.305, P=0.005), between POU2F3 and PD-L1 TPS (rho=0.297, P=0.006), between POU2F3 and PD-L1 CPS (rho=0.222, P=0.04), and between YAP1 and PD-L1 TPS (rho=0.349, P=0.001). (H-I) Expression levels of MHC I were positively associated with PD-L1 TPS (rho=0.239, P=0.03) and PD-L1 CPS (rho=0.433, P<0.001). (J) Representative images of a case showing positive staining for POU2F3, PD-L1 and MHC I, with the expression of POU2F3, PD-L1 (TPS), and MHC I at 220, 80% and 170, respectively (magnification: ×400). MHC I, major histocompatibility complex class I; MHC II, major histocompatibility complex class II; PD-L1, programmed death-ligand; Rb, retinoblastoma; ASCL1, achaete-scute homologue 1; POU2F3, POU class 2 homeobox 3; YAP1, Yes-associated protein 1; TPS, the tumor proportion score; CPS, the combined positive score.

Table 3 Tumor immune microenvironment characteristics of small cell lung carcinoma with MHC I/II expression

Parameter	MHC I			MHC II		
	Negative	Positive	P value	Negative	Positive	P value
Tumor PD-L1 expression			0.005*			>0.99
Negative	35 (97.2)	35 (74.5)		56 (84.8)	14 (82.4)	
Positive	1 (2.8)	12 (25.5)		10 (15.2)	3 (17.6)	
Stroma PD-L1 expression			<0.001*			>0.99
Negative	25 (69.4)	14 (29.8)		31 (47.0)	8 (47.1)	
Positive	11 (30.6)	33 (70.2)		35 (53.0)	9 (52.9)	

Table 3 (*continued*)

Table 3 (*continued*)

Parameter	MHC I			MHC II		
	Negative	Positive	P value	Negative	Positive	P value
Rb expression			0.40			>0.99
Negative	32 (88.9)	45 (95.7)		61 (92.4)	16 (94.1)	
Positive	4 (11.1)	2 (4.3)		5 (7.6)	1 (5.9)	
CD3 immunophenotypes			0.12			0.16
Immune desert	5 (13.9)	7 (14.9)		10 (15.2)	2 (11.8)	
Immune excluded	25 (69.4)	23 (48.9)		41 (62.1)	7 (41.2)	
Immune inflamed	6 (16.7)	17(36.2)		15 (22.7)	8 (47.0)	
CD4 immunophenotypes			0.71			0.22
Immune desert	2 (5.6)	4 (8.5)		6 (9.1)	0 (0)	
Immune excluded	26 (72.2)	30 (63.8)		45 (68.2)	11 (64.7)	
Immune inflamed	8 (22.2)	13 (27.7)		15 (22.7)	6 (35.3)	
CD8 immunophenotypes			0.048*			0.17
Immune desert	13 (36.1)	8 (17.0)		18 (27.3)	3 (17.7)	
Immune excluded	14 (38.9)	16 (34.0)		26 (39.4)	4 (23.5)	
Immune inflamed	9 (25.0)	23 (49.0)		22 (33.3)	10 (58.8)	
CD20 immunophenotypes			0.50			0.41
Immune desert	16 (44.4)	17 (36.2)		28 (42.4)	5 (29.4)	
Immune excluded	20 (55.6)	30 (63.8)		38 (57.6)	12 (70.6)	
Immune inflamed	0 (0)	0 (0)		0 (0)	0 (0)	
CD68 immunophenotypes			0.72			0.25
Immune desert	4 (11.1)	3 (6.4)		7 (10.6)	0 (0)	
Immune excluded	13 (36.1)	20 (42.6)		25 (37.9)	8 (47.1)	
Immune inflamed	19 (52.8)	24 (51.0)		34 (51.5)	9 (52.9)	
TLS			0.52			0.45
Absent	6 (16.7)	5 (10.6)		10 (15.2)	1 (5.9)	
Present	30 (83.3)	42 (89.4)		56 (84.8)	16 (94.1)	
Intra-TLS density			0.22			0.78
Low	29 (80.6)	32 (68.1)		48 (72.7)	13 (76.5)	
High	7 (19.4)	15 (31.9)		18 (27.3)	4 (23.5)	
Peri-TLS density			0.27			0.79
Low	21 (58.3)	21 (44.7)		34 (51.5)	8 (47.1)	
High	15 (41.7)	26 (55.3)		32 (48.5)	9 (52.9)	

Data are presented as n (%). *, significant P values. MHC I, major histocompatibility complex class I; MHC II, major histocompatibility complex class II; SCLC, small cell lung carcinoma; PD-L1, programmed death-ligand; Rb, retinoblastoma; TLS, tertiary lymphoid structure; intra-TLS, intra-tumoral tertiary lymphoid structure; peri-TLS, peri-tumoral tertiary lymphoid structure.

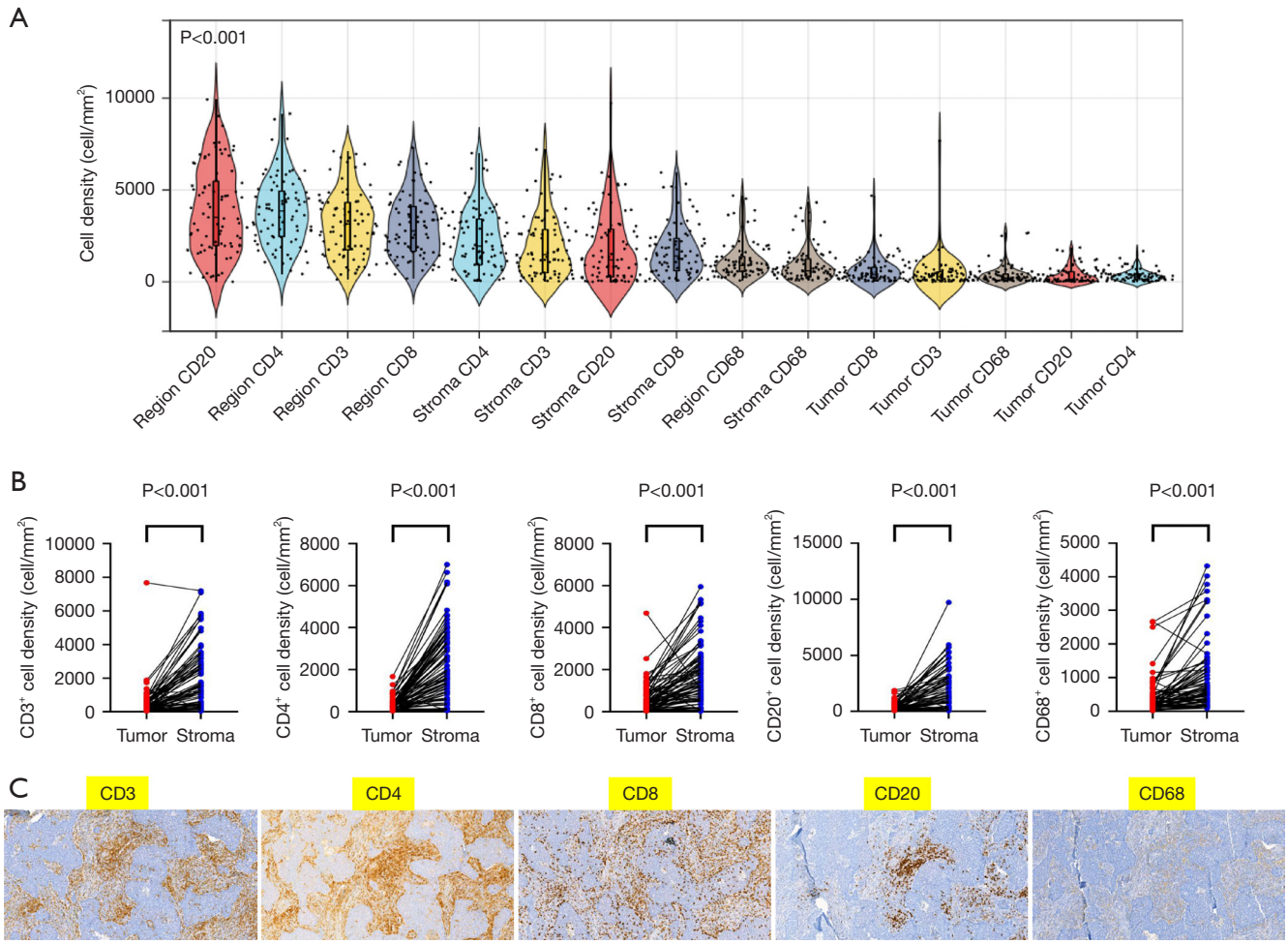

Figure 4 Immune cells infiltration density and spatial distribution. (A) Digital pathology quantification of CD3, CD4, CD8, CD20, and CD68 expressions revealed that in the TIME of resected SCLC, immune cells density was highest in the invasive margin of the tumors, with relatively few immune cells in the tumor interior. Among these, region CD20$^+$ B cells exhibited the highest density, followed by region CD4$^+$ T cells. In contrast, tumor-associated CD20$^+$ B cells and CD4$^+$ T cells showed relatively lower infiltration. (B) The density of all immune markers in the SCLC tumor stroma was higher than in the tumor interior. (C) Representative histopathological images demonstrated a higher extent of immune cell infiltration in the tumor stroma compared to the tumor nests (magnification: ×100). SCLC, small cell lung carcinoma; TIME, tumor immune microenvironment.

correlations were present between MHC II expression and tumor CD3 cell density, and between MHC II expression and tumor CD4 cell density, while no significant correlations were detected between other immune marker density and MHC I/II expression (Figure S5). Furthermore, when we grouped all tumors based on the median immune cells density, we found that high expression of stromal CD4$^+$ T cells was more commonly associated with the SCLC-A subtype (*Table 2*, Table S2).

The number and distribution of TLSs

TLSs were identified through immunostaining of CD20 and CD3. We quantified the number of TLSs across whole-slide images and assessed their location. A total of 80 cases exhibited TLSs, with intra-TLS and peri-TLS present in 50 (60.2%) and 80 (96.4%) patients, respectively. Notably, high intra-TLS density was more frequently observed in tumors of the SCLC-P subtype (P=0.02) (*Table 2*). However, neither the presence of TLSs nor the density of peri-

TILs was associated with the molecular subtypes of SCLC (*Table 2*).

Survival analysis in relation to clinicopathologic parameters including molecular subtypes and TIME features

All patients were routinely followed up. By the follow-up deadline of 31 May 2024, 51 cases (61.4%) had experienced tumor recurrence or metastasis, 26 (31.3%) were disease-free, 56 (67.5%) had died, 21 (25.3%) were alive, and 6 (7.2%) were lost to follow-up. The median OS and PFS were 44 and 31 months, respectively. To assess the prognostic value of molecular subtypes, TIME features, and other clinicopathologic parameters, we conducted univariate Cox regression analyses, and the results are summarized in Table S3. In the univariable analysis, male sex (P=0.003), TNM stage I (P=0.03), and low peri-TLS density (P<0.001) were significantly associated with better survival outcomes. Additionally, male sex (P=0.02), stromal PD-L1 expression (P=0.02), low tumor CD4 density (P=0.03), low region CD20 density (P=0.04), low tumor CD20 density (P=0.04), and low peri-TLS density (P=0.048) were significantly associated with longer PFS.

Next, clinicopathologic parameters with statistically significant differences in univariate analyses were included in a multivariate Cox proportional hazards regression model. The multivariable Cox analysis confirmed the independent prognostic roles of TNM stage, tumor CD4 density, and peri-TLS density for OS, and stromal PD-L1 expression for PFS (*Figure 5A*,*5B*).

Furthermore, Kaplan-Meier analysis was performed to compare risk stratification in subgroups according to these prognostic factors, included in the multivariate analysis (*Figure 5C*, Figure S6). The results showed that, in addition to sex and peri-TLS density, which were independent prognostic factors in this cohort, early TNM stage (I) was a predictive factor for OS. Stromal PD-L1 expression, low tumor CD4 density, low region CD20 density, and low tumor CD20 density were associated with longer PFS (*Figure 5C*). Kaplan-Meier curves for OS and PFS according to molecular subtypes were examined, but no significant differences were found among molecular subtypes (Figure S6).

Discussion

The clinical outlook for immunotherapy in SCLC remains challenging, with no reliable predictive biomarkers identified to date. Evaluating the TIME and specific immune signatures in SCLC is a critical step toward improving the efficacy of current immunotherapeutic strategies. While molecular subtypes of SCLC have been proposed, their clinical relevance and the therapeutic implications of TIME are not yet fully understood. In this study, we investigated the protein expression profiles of molecular subtype markers and analyzed the immunological landscape of SCLC by assessing the expression pattern of nine immune-related markers in surgically resected SCLC tumors.

No YAP1 subtype was identified in our cohort, which is in consistent with most reports (9-12,33). Similarly, our unsupervised hierarchal clustering analyses identified a new SCLC subtype, SCLC-QN, characterized by the low expression of all four subtype-specific proteins. Although SCLC-QN ($NAPY^-$) tumors shared some similarities with the SCLC-I subtype as reported by Gay *et al.* (9), they were classified based on different tumor transcriptome data. Recent studies have shown that the inflamed phenotype in SCLC is not exclusive to a specific subtype, but rather varies in prevalence across molecular subtypes (17). In our study, we found that the inflamed phenotype of $CD8^+$ T cells and $CD3^+$ T cells was more commonly observed in the SCLC-P subtype than in other molecular subtypes (P=0.001 and P=0.003). Previous research has demonstrated that tumor-associated $CD8^+$ T-cells play a role in cytotoxic killing and are associated with clinical responses to ICI in relapsed SCLC (34). In line with the findings of Chen *et al.* (15), we speculate that SCLC-P subtype could serve as a predictive biomarker for ICIs response in SCLC. Further investigation is needed to understand the mechanisms by which POU2F3, a key transcriptional regulator, influences immune regulation in SCLC.

In addition, we found that the expression rates of both MHC I and MHC II on tumor cells in the SCLC-P subtype were significantly higher compared to other molecular subtypes (P=0.02, P=0.02). Furthermore, the expression level of MHC II on tumor cells in the SCLC-P subtype was the highest among the four molecular subtypes (P=0.04). These findings suggest that tumors with the SCLC-P subtype may recruit T cells via MHC I/II, a hypothesis that warrants further clinical validation. Notably, the CASPIAN trial demonstrated longer OS in SCLC patients with MHC II expression who received durvalumab plus tremelimumab in combination with etoposide and platinum chemotherapy (35). When combined with our analysis of PD-L1 expression,

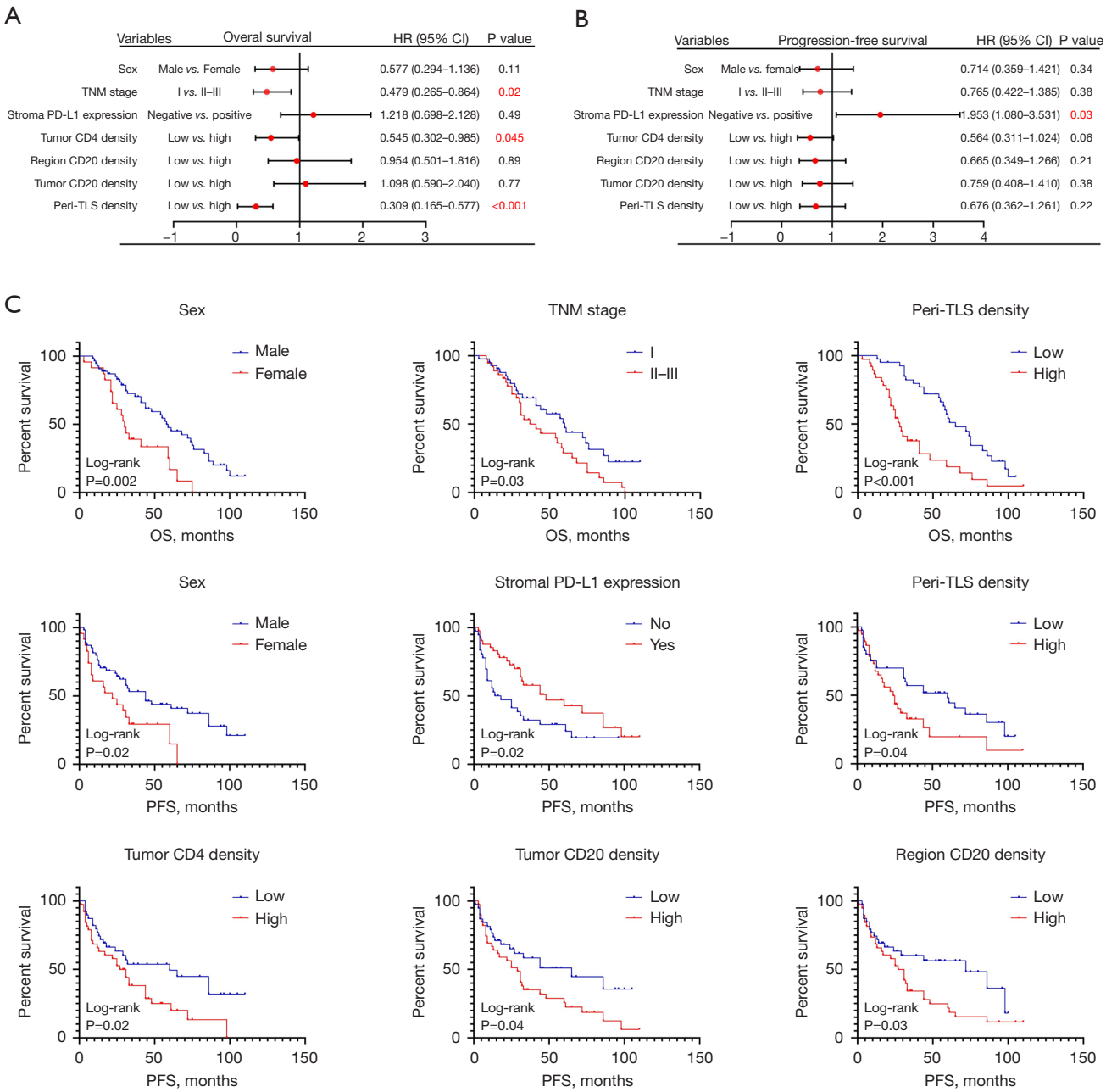

Figure 5 Survival analysis in relation to clinicopathologic parameters including molecular subtypes and TIME features. (A,B) Multivariable Cox analysis identified TNM stage, tumor CD4 density, peri-TLS density, and stromal PD-L1 expression as independent prognostic factors for OS and PFS. (C) Kaplan-Meier analysis was used to compare the risk stratification of subgroups based on these prognostic factors, which were included in the multivariate analysis. The results showed that, in addition to sex and peri-TLS density, which were independent prognostic factors in the cohort, early TNM stage (Stage I) was predictive of better OS, while stromal PD-L1 expression, low tumor CD4 density, low region CD20 density and low tumor CD20 density were associated with longer PFS. TIME, tumor immune microenvironment; peri-TLS, peri-tumoral tertiary lymphoid structure; OS, overall survival; PFS, progression-free survival; TNM, tumor-node-metastasis.

which revealed higher PD-L1 levels in patients with SCLC-P subtype and MHC I expression, it is likely that these patients could benefit more from ICIs treatment. Collectively, these results suggest that the SCLC-P subtype and tumor MHC I expression may serve as potential predictors of immunotherapy efficacy in SCLC patients, although further validation through larger, prospective studies is required.

Previous studies have reported that NE-low SCLC is characterized by greater T cell infiltration compared to NE-high SCLC (27,36,37). Additionally, recent studies have shown that T cell scores are highest in the POU2F3 subtype, which also exhibits elevated expression of immune-related genes (14). Among the 10 genes used to predict SCLC-I, POU2F3 was the most significantly upregulated with high expression (15). However, Nabet *et al.* recently presented a contrasting view, suggesting that NE-high tumors with high T cell and low macrophage infiltration benefit from anti-PD-L1 combined with chemotherapy (16). Furthermore, it has been reported that patients with the SCLC-A/N subtype had similar PFS compared to non-SCLC-A/N patients following treatment with ICIs plus chemotherapy (38). These findings suggest that the current binary classification of SCLC into NE-high and NE-low is insufficient. There is an urgent need for a comprehensive analysis of immune cells status in the TIME of each molecular subtype, including the identification of immune cells subtypes, their proportions, density, distribution, and spatial relationships with tumor cells.

Consistent with previously published data, most SCLC tumors exhibited diffuse staining for $CD3^+$ T cells (39), with $CD3^+$, $CD4^+$, and $CD8^+$ tumor-infiltrating T lymphocytes primarily localized within the tumor stroma (40,41). Additionally, we observed that the density of $CD20^+$ B cells and $CD68^+$ macrophages was higher in the tumor stroma than in the tumor interior. This supports the idea that the microenvironments of the tumor parenchyma and stroma are differently constructed, resulting in distinct anti-tumor immune responses (42). Notably, we found the highest immune cell density at the leading edge of the tumors, with relatively few immune cells within the tumor core. The higher density of $CD20^+$ B cells and $CD4^+$ T cells at the invasive margin may partly explain the lower immune cell infiltration in the tumor core, potentially contributing to the immunosuppressive mechanism observed in SCLC. To further understand the characteristics and mechanisms underlying the spatial distribution of these immune cells, more advanced techniques such as multiplex IHC and single-cell RNA sequencing, and spatial transcriptomics will be essential in future studies.

It has been reported that TLSs provide a crucial microenvironment for both cellular and humoral immune responses against tumor cells and are present in various types of cancer (43,44). To our knowledge, this is the first study to evaluate the presence and location of TLSs *in situ* with SCLC whole tissue samples from a relatively large patient cohort. Our results the number of peri-TILs was significantly higher than intra-TLSs (96.4% *vs.* 60.2%). Notably, high intra-TLS density was more frequently observed in tumors of the SCLC-P subtype (P=0.02). Given that the expression rate of MHC I and MHC II on tumor cells in the SCLC-P subtype were the highest compared to other molecular subtypes, we hypothesize that intra-TLSs may contribute to effective anti-tumor immune responses by promoting local antigen presentation and lymphocyte differentiation. However, the specific roles and underlying mechanisms of TLSs in this context require further investigation.

Moreover, recent studies have suggested that TLSs are associated with favorable clinical outcomes in various malignancies (43,45). However, we did not observe a prognostic significance for intra-TILs in our study. This discrepancy may be partly explained by the relatively low incidence of high intra-TLS density (22/83, 26.5%). Our survival analysis indicated that patients with high peri-TLS density had significantly poorer OS in both univariable and multivariable Cox analyses. These findings align with those of Gong *et al.*, who reported that high peri-TLS density was associated with worse survival in patients with combined hepatocellular-cholangiocarcinoma (32). To validate the prognostic significance of TLSs in our study, further multicenter prospective research is needed.

Another important finding in our study is the independent prognostic role of stromal immune cells with PD-L1 expression for PFS, as demonstrated by multivariable Cox analysis. This suggests that PD-L1 expression on stromal immune cells reflects the presence of *in situ*, effective anti-tumor immunity. Supporting this, previous studies have shown that PD-L1 expression is predominantly present on inflammatory cells and serves as an indicator of favorable prognosis for SCLC patients (46-49). Therefore, CPS could serve as an alternative method for evaluating PD-L1 expression in SCLC. Although the definition of CPS is more complex than the TPS, CPS has been widely used in PD-L1 evaluation across various cancer types. More evidence is needed to validate the utility of

CPS in predicting response to ICIs in SCLC, and further research is required to explore the underlying molecular mechanisms.

There are limitations in this study. First, it was a retrospective and single-center study, which inherently introduces selection bias. Second, although we managed to collect a relatively large number of surgically resected SCLC samples for immune landscape analysis, the overall sample size remains modest. Third, exploring the direct effects of immunotherapy is not feasible in this study, as we only included surgically treated, limited-stage SCLC patients who did not receive ICIs as part of their standard treatment. Whether the SCLC-P subtype and MHC I expression can serve as predictive biomarkers for immunotherapy efficacy will require validation in future clinical trials. Lastly, conventional IHC was employed in this study; more advanced, information-rich techniques such as multiplex IHC, single-cell sequencing, and spatial transcriptome analysis will be needed to further explore the spatial distribution and underlying mechanisms of immune cell infiltration. Nevertheless, by utilizing whole-slide image-based digital pathology, our results are hypothesis-generating and provide a foundation for future studies aiming to validate these findings.

Conclusions

In summary, our study highlights the heterogeneity of the TIME across different molecular subtypes of SCLC. We found that the SCLC-P subtype and MHC I expression may be predictive markers for the efficacy of immunotherapy. Additionally, the stroma of SCLC tumors exhibited significantly higher immune cell infiltration than the tumor interior, with the highest density of $CD20^+$ B cells and $CD4^+$ T cells observed in the tumor's invasive margin. This pattern may play a role in the immunosuppressive mechanism of SCLC. Moreover, low peri-TLS density was associated with better survival outcomes. Multivariable Cox analysis further supported the independent prognostic value of stromal immune cells expressing PD-L1 for PFS, suggesting that these cells contribute to anti-tumor immunity. Furthermore, the CPS could be a useful alternative for evaluating PD-L1 expression in SCLC.

Acknowledgments

None.

Footnote

Reporting Checklist: The authors have completed the REMARK reporting checklist. Available at https://tlcr.amegroups.com/article/view/10.21037/tlcr-24-924/rc

Data Sharing Statement: Available at https://tlcr.amegroups.com/article/view/10.21037/tlcr-24-924/dss

Peer Review File: Available at https://tlcr.amegroups.com/article/view/10.21037/tlcr-24-924/prf

Funding: This work was supported by the Science Foundation of Peking University Cancer Hospital (PY202303).

Conflicts of Interest: All authors have completed the ICMJE uniform disclosure form (available at https://tlcr.amegroups.com/article/view/10.21037/tlcr-24-924/coif). The authors have no conflicts of interest to declare.

Ethical Statement: The authors are accountable for all aspects of the work in ensuring that questions related to the accuracy or integrity of any part of the work are appropriately investigated and resolved. This study was approved by the Ethics Committee of Peking University Cancer Hospital (2023KT23). Given the retrospective design, informed consent from patients was not required, and all patient data were kept confidential. The study was conducted in accordance with the Declaration of Helsinki (as revised in 2013).

References

1. Rudin CM, Brambilla E, Faivre-Finn C, et al. Small-cell lung cancer. Nat Rev Dis Primers 2021;7:3.
2. Horn L, Mansfield AS, Szczęsna A, et al. First-Line

Atezolizumab plus Chemotherapy in Extensive-Stage Small-Cell Lung Cancer. N Engl J Med 2018;379:2220-9.
3. Paz-Ares L, Dvorkin M, Chen Y, et al. Durvalumab plus platinum-etoposide versus platinum-etoposide in first-line treatment of extensive-stage small-cell lung cancer (CASPIAN): a randomised, controlled, open-label, phase 3 trial. Lancet 2019;394:1929-39.
4. Liu SV, Reck M, Mansfield AS, et al. Updated Overall Survival and PD-L1 Subgroup Analysis of Patients With Extensive-Stage Small-Cell Lung Cancer Treated With Atezolizumab, Carboplatin, and Etoposide (IMpower133). J Clin Oncol 2021;39:619-30.
5. Paz-Ares L, Chen Y, Reinmuth N, et al. Durvalumab, with or without tremelimumab, plus platinum-etoposide in first-line treatment of extensive-stage small-cell lung cancer: 3-year overall survival update from CASPIAN. ESMO Open 2022;7:100408.
6. Li T, Qiao T. Unraveling tumor microenvironment of small-cell lung cancer: Implications for immunotherapy. Semin Cancer Biol 2022;86:117-25.
7. Rudin CM, Poirier JT, Byers LA, et al. Molecular subtypes of small cell lung cancer: a synthesis of human and mouse model data. Nat Rev Cancer 2019;19:289-97.
8. Tian Y, Li Q, Yang Z, et al. Single-cell transcriptomic profiling reveals the tumor heterogeneity of small-cell lung cancer. Signal Transduct Target Ther 2022;7:346.
9. Gay CM, Stewart CA, Park EM, et al. Patterns of transcription factor programs and immune pathway activation define four major subtypes of SCLC with distinct therapeutic vulnerabilities. Cancer Cell 2021;39:346-360.e7.
10. Baine MK, Hsieh MS, Lai WV, et al. SCLC Subtypes Defined by ASCL1, NEUROD1, POU2F3, and YAP1: A Comprehensive Immunohistochemical and Histopathologic Characterization. J Thorac Oncol 2020;15:1823-35.
11. Megyesfalvi Z, Barany N, Lantos A, et al. Expression patterns and prognostic relevance of subtype-specific transcription factors in surgically resected small-cell lung cancer: an international multicenter study. J Pathol 2022;257:674-86.
12. Hwang S, Hong TH, Kim HK, et al. Whole-Section Landscape Analysis of Molecular Subtypes in Curatively Resected Small Cell Lung Cancer: Clinicopathologic Features and Prognostic Significance. Mod Pathol 2023;36:100184.
13. Goldman JW, Dvorkin M, Chen Y, et al. Durvalumab, with or without tremelimumab, plus platinum-etoposide versus platinum-etoposide alone in first-line treatment of extensive-stage small-cell lung cancer (CASPIAN): updated results from a randomised, controlled, open-label, phase 3 trial. Lancet Oncol 2021;22:51-65.
14. Best SA, Hess JB, Souza-Fonseca-Guimaraes F, et al. Harnessing Natural Killer Immunity in Metastatic SCLC. J Thorac Oncol 2020;15:1507-21.
15. Chen Y, Fang Z, Tang Y, et al. Integrative analysis of multi-omics data reveals the heterogeneity and signatures of immune therapy for small cell lung cancer. Clin Transl Med 2021;11:e620.
16. Nabet BY, Hamidi H, Lee MC, et al. Immune heterogeneity in small-cell lung cancer and vulnerability to immune checkpoint blockade. Cancer Cell 2024;42:429-443.e4.
17. Park S, Hong TH, Hwang S, et al. Comprehensive analysis of transcription factor-based molecular subtypes and their correlation to clinical outcomes in small-cell lung cancer. EBioMedicine 2024;102:105062.
18. Nguyen EM, Taniguchi H, Chan JM, et al. Targeting Lysine-Specific Demethylase 1 Rescues Major Histocompatibility Complex Class I Antigen Presentation and Overcomes Programmed Death-Ligand 1 Blockade Resistance in SCLC. J Thorac Oncol 2022;17:1014-31.
19. Alspach E, Lussier DM, Miceli AP, et al. MHC-II neoantigens shape tumour immunity and response to immunotherapy. Nature 2019;574:696-701.
20. Yarchoan M, Albacker LA, Hopkins AC, et al. PD-L1 expression and tumor mutational burden are independent biomarkers in most cancers. JCI Insight 2019;4:e126908.
21. Dowlati A, Abbas A, Chan T, et al. Immune Checkpoint Blockade Outcome in Small-Cell Lung Cancer and Its Relationship With Retinoblastoma Mutation Status and Function. JCO Precis Oncol 2022;6:e2200257.
22. Väyrynen JP, Vornanen JO, Sajanti S, et al. An improved image analysis method for cell counting lends credibility to the prognostic significance of T cells in colorectal cancer. Virchows Arch 2012;460:455-65.
23. Pagès F, Berger A, Camus M, et al. Effector memory T cells, early metastasis, and survival in colorectal cancer. N Engl J Med 2005;353:2654-66.
24. Goldstraw P, Chansky K, Crowley J, et al. The IASLC Lung Cancer Staging Project: Proposals for Revision of the TNM Stage Groupings in the Forthcoming (Eighth) Edition of the TNM Classification for Lung Cancer. J Thorac Oncol 2016;11:39-51.
25. Zhu Y, Li S, Wang H, et al. Molecular subtypes, predictive markers and prognosis in small-cell lung carcinoma. J Clin

Pathol 2024;78:42-50.
26. Fedchenko N, Reifenrath J. Different approaches for interpretation and reporting of immunohistochemistry analysis results in the bone tissue - a review. Diagn Pathol 2014;9:221.
27. Qu S, Fetsch P, Thomas A, et al. Molecular Subtypes of Primary SCLC Tumors and Their Associations With Neuroendocrine and Therapeutic Markers. J Thorac Oncol 2022;17:141-53.
28. Iams WT, Porter J, Horn L. Immunotherapeutic approaches for small-cell lung cancer. Nat Rev Clin Oncol 2020;17:300-12.
29. Kulangara K, Zhang N, Corigliano E, et al. Clinical Utility of the Combined Positive Score for Programmed Death Ligand-1 Expression and the Approval of Pembrolizumab for Treatment of Gastric Cancer. Arch Pathol Lab Med 2019;143:330-7.
30. Bankhead P, Loughrey MB, Fernández JA, et al. QuPath: Open source software for digital pathology image analysis. Sci Rep 2017;7:16878.
31. Mariathasan S, Turley SJ, Nickles D, et al. TGFβ attenuates tumour response to PD-L1 blockade by contributing to exclusion of T cells. Nature 2018;554:544-8.
32. Gong W, Zhang S, Tian X, et al. Tertiary lymphoid structures as a potential prognostic biomarker for combined hepatocellular-cholangiocarcinoma. Hepatol Int 2024;18:1310-25.
33. Go SI, Yang JW, Jeong EJ, et al. Redefining YAP1 in small cell lung cancer: shifting from a dominant subtype marker to a favorable prognostic indicator. Transl Lung Cancer Res 2024;13:1768-79.
34. Thomas A, Vilimas R, Trindade C, et al. Durvalumab in Combination with Olaparib in Patients with Relapsed SCLC: Results from a Phase II Study. J Thorac Oncol 2019;14:1447-57.
35. Garassino M, Shrestha Y, Xie M, et al. MA16.06 Durvalumab ± Tremelimumab + Platinum-Etoposide in 1L ES-SCLC: Exploratory Analysis of HLA Genotype and Survival in CASPIAN. J Thorac Oncol 2021;16:S939.
36. Dora D, Rivard C, Yu H, et al. Neuroendocrine subtypes of small cell lung cancer differ in terms of immune microenvironment and checkpoint molecule distribution. Mol Oncol 2020;14:1947-65.
37. Cai L, Liu H, Huang F, et al. Cell-autonomous immune gene expression is repressed in pulmonary neuroendocrine cells and small cell lung cancer. Commun Biol 2021;4:314.
38. Chiang CL, Huang HC, Luo YH, et al. Clinical utility of immunohistochemical subtyping in patients with small cell lung cancer. Lung Cancer 2024;188:107473.
39. Zhao X, Kallakury B, Chahine JJ, et al. Surgical Resection of SCLC: Prognostic Factors and the Tumor Microenvironment. J Thorac Oncol 2019;14:914-23.
40. Wang W, Hodkinson P, McLaren F, et al. Small cell lung cancer tumour cells induce regulatory T lymphocytes, and patient survival correlates negatively with FOXP3+ cells in tumour infiltrate. Int J Cancer 2012;131:E928-37.
41. Wang H, Li Z, Dong B, et al. Prognostic significance of PD-L1 expression and CD8+ T cell infiltration in pulmonary neuroendocrine tumors. Diagn Pathol 2018;13:30.
42. Binnewies M, Roberts EW, Kersten K, et al. Understanding the tumor immune microenvironment (TIME) for effective therapy. Nat Med 2018;24:541-50.
43. Fridman WH, Zitvogel L, Sautès-Fridman C, et al. The immune contexture in cancer prognosis and treatment. Nat Rev Clin Oncol 2017;14:717-34.
44. Schumacher TN, Thommen DS. Tertiary lymphoid structures in cancer. Science 2022;375:eabf9419.
45. Dieu-Nosjean MC, Giraldo NA, Kaplon H, et al. Tertiary lymphoid structures, drivers of the anti-tumor responses in human cancers. Immunol Rev 2016;271:260-75.
46. Sun C, Zhang L, Zhang W, et al. Expression of PD-1 and PD-L1 on Tumor-Infiltrating Lymphocytes Predicts Prognosis in Patients with Small-Cell Lung Cancer. Onco Targets Ther 2020;13:6475-83.
47. Zhu L, Cheng G, Wu M, et al. Heterogeneous distribution pattern of CD3+ tumor-infiltrated lymphocytes (TILs) and high combined positive score (CPS) favored the prognosis of resected early stage small-cell lung cancer. Transl Oncol 2023;34:101697.
48. Kasajima A, Ishikawa Y, Iwata A, et al. Inflammation and PD-L1 expression in pulmonary neuroendocrine tumors. Endocr Relat Cancer 2018;25:339-50.
49. Carvajal-Hausdorf D, Altan M, Velcheti V, et al. Expression and clinical significance of PD-L1, B7-H3, B7-H4 and TILs in human small cell lung Cancer (SCLC). J Immunother Cancer 2019;7:65.

Cite this article as: Zhu Y, Wu J, Wang H, Chi K, Diao X, Zhuo M, Lin D. Whole-section digital analysis of immune profiles in surgically resected small cell lung carcinoma and their associations with molecular subtypes. Transl Lung Cancer Res 2025;14(2):449-466. doi: 10.21037/tlcr-24-924

